Available online at www.sciencedirect.com
SCIENCE DIRECT®
Journal of Computational Physics 201 (2004) 487–510
JOURNAL OF COMPUTATIONAL PHYSICS
www.elsevier.com/locate/jcp

Domain decomposition method for dynamic faulting under slip-dependent friction

Lori Badea [a], Ioan R. Ionescu [b,*], Sylvie Wolf [b,c]

[a] *Institute of Mathematics of the Romanian Academy, P.O. Box 1-764, RO 70700, Bucharest, Romania*
[b] *Laboratoire de Mathématiques, Université de Savoie, Campus Scientifique, 73376 Le Bourget-du-Lac Cedex, France*
[c] *Laboratoire de Géophysique Interne et Tectonophysique, Université Joseph Fourier, BP 53X, 38041 Grenoble Cedex, France*

Received 31 December 2003; received in revised form 8 June 2004; accepted 8 June 2004
Available online 20 July 2004

Abstract

The anti-plane shearing problem on a system of finite faults under a slip-dependent friction in a linear elastic domain is considered. Using a Newmark method for the time discretization of the problem, we have obtained an elliptic variational inequality at each time step. An upper bound for the time step size, which is not a CFL condition, is deduced from the solution uniqueness criterion using the first eigenvalue of the tangent problem. Finite element form of the variational inequality is solved by a Schwarz method assuming that the inner nodes of the domain lie in one subdomain and the nodes on the fault lie in other subdomains. Two decompositions of the domain are analyzed, one made up of two subdomains and another one with three subdomains. Numerical experiments are performed to illustrate convergence for a single time step (convergence of the Schwarz algorithm, influence of the mesh size, influence of the time step), convergence in time (instability capturing, energy dissipation, optimal time step) and an application to a relevant physical problem (interacting parallel fault segments).

AMS: 65M55; 65N55; 74L05; 74S05; 86A15; 86A17

Keywords: Domains with cracks; Slip-dependent friction; Wave equation; Earthquake initiation; Domain decomposition methods; Schwarz method

1. Introduction

Since no direct observation is available, numerical modeling is an important tool in the understanding of earthquake phenomena. In the last decade significant progress was achieved in improving inversion techniques as well as in developing numerical methods for direct computations.

* Corresponding author. Tel.: +33-479-758-642; fax: +33-479-758-142.
E-mail addresses: lori.badea@imar.r (L. Badea), ionescu@univ-savoie.fr (I.R. Ionescu), swolf@univ-savoie.fr (S. Wolf).

0021-9991/$ - see front matter © 2004 Elsevier Inc. All rights reserved.
doi:10.1016/j.jcp.2004.06.003

In numerical modeling of the earthquake source dynamics (initiation, rupture propagation and arrest) we need accurate and robust numerical schemes. Two methods have been widely used: boundary integral methods [5,14,18,19,25,27] and finite difference methods [13,35,43,52]. Finite element models [1,4,44] are much fewer in earthquake rupture simulation, because they are more difficult to implement than finite differences, and because low order schemes can lead to undesirable dissipation. However, they have been more and more used because they can handle strong heterogeneities as well as complex geometries [45,46]. A special case of finite elements, called spectral elements (see [12]), combines high order precision and geometrical flexibility. The papers [38–40] validated the use of spectral elements for 3D wave propagation. Applications in the propagation of seismic rupture are investigated in [2]. Also, even if it does not deal with rupture propagation, we have to mention here the model of [10,11,50], built for the propagation of 3D elastic waves in a medium containing (stress free) cracks: it is based on a new class of mixed finite elements and it uses the fictitious domain method to couple a regular mesh in the medium and an irregular mesh on the cracks, using Lagrange multipliers.

The earthquake nucleation (or initiation) phase, preceding the dynamic rupture, has been recently pointed out by detailed seismological observations [22,34], laboratory experiments on friction [47] and by theoretical studies [3,15,21,35,51]. Since the initiation phase is characterized by an unstable evolution with an exponential growth in time, the behavior of the solution was described, as it is here, by its "dominant part" through an eigenvalue analysis [15,20,21,23,24]. Only few numerical schemes can capture this unstable behavior of the solution during the initiation phase. One of them was proposed in [35], for the anti-plane problem, and developed thereafter in [23,24] for the in-plane and 3D problems, but the use of a finite difference method restricts the applications on the planar fault geometries.

The aim of this paper is to propose a numerical scheme able to describe the initiation and the rupture propagation on a fault system with a complex geometry and to handle heterogeneous material and frictional properties. The duration of the initiation phase may be very large [15,21,35] and it may not scale with the characteristic time of the wave equation (i.e. characteristic length/wave speed). That is why we need an implicit time discretization scheme with a much larger time step than the critical CFL time step. The use of an implicit scheme for the wave equation with frictional type conditions on the faults will imply that we have to solve a nonlinear problem, given by a variational inequality, at each time step. We propose in this paper a domain decomposition method for the solution of this variational inequality.

The domain decomposition methods have received considerable attention in the past decades, and the literature on them is too large to survey here. We can refer, for instance, to the papers in the proceedings of the 15 annual conferences on domain decomposition methods starting in 1988 with [28]. Also, we can refer to the bibliography given in the papers [16,41,54], or that in the books [48,49]. The variational inequality in our problem comes from the constraint minimization over a convex set of a non-quadratic functional. Besides, the convex set is not of an obstacle type, for which most of the convergence results are given in the literature. The domain decomposition method we propose to solve our problem is of the multiplicative Schwarz type, and it has been introduced in [6], where the convergence has been proved for the minimization of quadratic functionals. This method has been extended to one- and two-level methods in [8]. Also, its convergence for the constraint minimization of the non-quadratic convex functionals in a reflexive Banach space is proved in [7]. Using the general convergence theorem in [7], error estimates are given in [9] for the one-, two- and multilevel methods, when they are applied to the solution of the variational inequalities coming from the constraint minimization of the non-quadratic functionals over enough general convex sets.

Let us give here the sketch of the paper. In Section 2 we consider the anti-plane shearing on a system of finite faults under a slip-dependent friction in a linear elastic domain. The system describes a shear crack propagating on a pre-existing surface of weakness in a linearly elastic solid, with slip driven by a stress drop. A Newmark method for the time discretization is used to deduce an elliptic variational inequality at each time step. In order to have uniqueness of this nonlinear problem, an upper bound of the time step size

is deduced using the first eigenvalue of the tangent problem. In all the physical applications we have considered, this restriction, which is not a CFL-type condition, gives large critical time steps (10 up to 100 times larger than the critical CFL time step). On the basis of a finite element space discretization we present the Schwarz algorithm we use to solve the variational inequality. Using an overlapping decomposition with two or three subdomains, we solve in each iteration an algebraic linear system corresponding to the inner nodes of the domain, and some small nonlinear problems, of two unknowns, corresponding to the nodes on the fault. Numerical results, presented in Section 5, include convergence tests for a single time step (influence of the mesh size, convergence of the Schwarz algorithm, influence of the time step), convergence in time (instability capturing, energy dissipation, optimal time step) and an application to a relevant physical problem (interacting parallel fault segments).

2. Problem statement

Consider, as in [20,21,51], the anti-plane shearing on a system of finite faults under a slip-dependent friction in a linear elastic domain, to describe a shear crack propagating on a pre-existing surface of weakness with slip driven by a stress drop. Let $\Omega \subset \mathbb{R}^2$ be a domain, not necessarily bounded, containing a finite number of cuts. Its boundary $\partial\Omega$ is supposed to be smooth and divided into two disjoint parts: the exterior boundary $\Gamma_d = \partial\bar{\Omega}$ and the internal one Γ composed of N_f bounded connected arcs Γ_f^i, $i = 1, \ldots, N_f$, called cracks or faults. We suppose that the displacement field $u = (u_1, u_2, u_3)$ is 0 in directions Ox_1 and Ox_2 and that u_3 does not depend on x_3. The displacement is therefore denoted simply by $w = w(t, x_1, x_2)$. A schematic representation of the antiplane shearing of a single finite fault lying on Ox_1 is plotted in Fig. 1. The elastic medium has the shear rigidity G, the density ρ and the shear velocity $c = \sqrt{G/\rho}$ with the following regularity:

$$\rho, G \in L^\infty(\Omega), \quad \rho(x) \geqslant \rho_0 > 0, \quad G(x) \geqslant G_0 > 0 \quad \text{a.e. } x \in \Omega.$$

The non-vanishing shear stress components are $\sigma_{31} = \tau_1^\infty + G\partial_1 w$, $\sigma_{32} = \tau_2^\infty + G\partial_2 w$, and $\sigma_{11} = \sigma_{22} = -S$, where τ^∞ is the pre-stress and $S > 0$ is the normal stress on the faults, such that

$$S, \tau_1^\infty, \tau_2^\infty \in C^0(\bar{\Omega}).$$

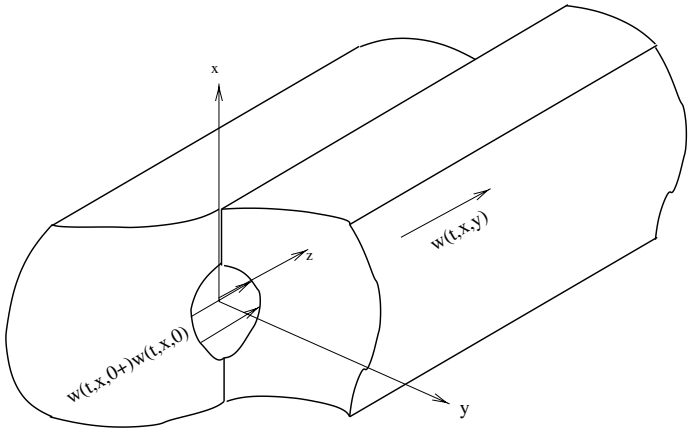

Fig. 1. The antiplane shearing of one finite fault.

On Γ we denote by [] the jump across Γ (i.e. $[w] = w^+ - w^-$) and by $\partial_n = \nabla \cdot n$ the corresponding normal derivative with the unit normal n outwards the positive side. We suppose that we can choose the orientation of the unit normal n of each connected fault (cut) of Γ such that

$$q(x) = \tau_1^\infty(x)n_1(x) + \tau_2^\infty(x)n_2(x) \leqslant q_0 < 0 \quad \text{a.e. } x \in \Gamma. \tag{1}$$

This is the case in many concrete applications, when the pre-stress τ^∞ gives a dominant direction of slip.

On the contact zone Γ we have

$$[G\partial_n w] = 0,$$

and we consider a slip-dependent friction law. The friction force is depending on the slip $[w]$ through a friction coefficient $\mu = \mu([w])$ which is multiplied by the normal stress S:

$$G\partial_n w + q = -\mu(|[w(t)]|)S\,\mathrm{sign}(\partial_t[w]) \quad \text{if } \partial_t[w] \neq 0, \tag{2}$$

$$|G\partial_n w + q| \leqslant \mu(|[w]|)S \quad \text{if } \partial_t[w] = 0. \tag{3}$$

The above equations assert that the tangential (frictional) stress is bounded by the normal stress S multiplied by the value of the friction coefficient μ. If such a limit is not attained sliding does not occur. Otherwise the friction stress is opposed to the slip rate $\partial_t[w]$ and its absolute value depends on the slip through μ. A generic representation of the nonlinear dependence of friction coefficient μ with respect to the relative slip is shown in Fig. 2.

Concerning the regularity of $\mu: \Gamma \times \mathbb{R}_+ \to \mathbb{R}$, we suppose that the friction coefficient is a Lipschitz function, with respect to the slip, and let f be

$$f(x,s) = S(x)\mu(x,s) + q(x).$$

We suppose that there exists $L > 0$, such that

$$|f(x,s_1) - f(x,s_2)| \leqslant L|s_1 - s_2| \tag{4}$$

a.e. $x \in \Gamma$, and for all $s_1, s_2 \in \mathbb{R}_+$.

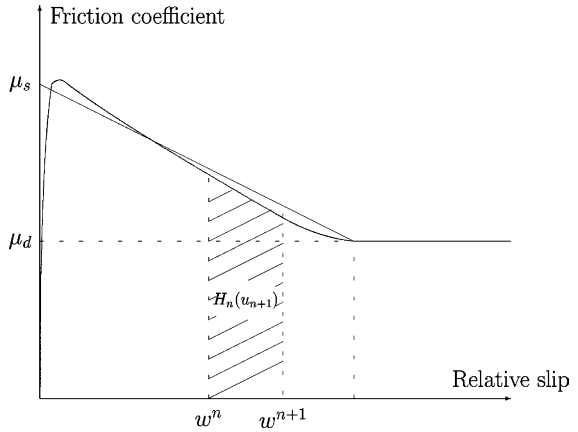

Fig. 2. A generic representation of the nonlinear dependence of friction coefficient μ with respect to the relative slip and its piecewise linear approximation.

In our numerical experiments, we used a piecewise linear friction law (see also Fig. 2) of the following form:

$$\begin{aligned} &\mu(x,u) = \mu_s(x) - \tfrac{\mu_s(x)-\mu_d(x)}{2D_c(x)}u \quad \text{if } u \leqslant 2D_c(x),\\ &\mu(x,u) = \mu_d(x) \qquad\qquad\qquad\quad \text{if } u > 2D_c(x), \end{aligned} \tag{5}$$

where u is the relative slip, μ_s and μ_d ($\mu_s > \mu_d$) are the static and dynamic friction coefficients, and D_c is the critical slip. This piecewise linear function is a reasonable approximation of the experimental observations reported by [47], and has been quite frequentely used. If we put

$$L = \sup_{x\in\Gamma} S(x)\frac{\mu_s(x)-\mu_d(x)}{2D_c(x)}, \tag{6}$$

then (4) holds. The numerical scheme proposed in this paper is designed to handle any arbitrary dependence of the friction force on the slip. Though the numerical experiments presented at the end of the paper are performed using the piecewise linear model, the algorithm does not use the linearity of the weakening law.

Since we are looking for dynamic perturbations of the equilibrium $w \equiv 0$, and since the slip direction is given by τ^∞ and q (see (1)), we can restrict the above friction law to the case of non-negative slip rate $\partial_t[w] \geqslant 0$. Since the initial slip can also be supposed non-negative, we have $[w(t)] \geqslant 0$ also. These are usual assumptions in the geophysical approach of earthquake source dynamics.

Using the above assumptions, the momentum balance law $\operatorname{div}\sigma = \rho\partial_{tt}u$ and the boundary conditions, we obtain the following dynamic problem (DP).

Find $w:\ \mathbb{R}_+ \times \Omega \to \mathbb{R}$, solution of the wave equation

$$\rho\partial_{tt}w(t) = \operatorname{div}(G\nabla w(t)) \quad \text{in } \Omega, \tag{7}$$

with boundary conditions of the Signorini type

$$w(t) = 0 \quad \text{on } \Gamma_d, \qquad [G\partial_n w(t)] = 0, \qquad [\partial_t w(t)] \geqslant 0 \quad \text{on } \Gamma \tag{8}$$

$$G\partial_n w(t) + f([w(t)]) \geqslant 0,\ \ [\partial_t w(t)](G\partial_n w(t) + f([w(t)])) = 0 \quad \text{on } \Gamma. \tag{9}$$

The initial conditions are

$$w(0) = w_0,\ \ \partial_t w(0) = w_1 \quad \text{in } \Omega. \tag{10}$$

Any solution of the above problem satisfies the following variational problem (VP).

Find $w:\ [0,T] \to V$ such that

$$\begin{aligned} &\partial_t w(t) \in W_+, \quad \int_\Omega \rho\partial_{tt}w(t)(v-\partial_t w(t))\mathrm{d}x + \int_\Omega G\nabla w(t)\cdot\nabla(v-\partial_t w(t))\mathrm{d}x\\ &\quad + \int_\Gamma f([w(t)])([v]-[\partial_t w(t)])\mathrm{d}\sigma \geqslant 0 \quad \forall v \in W_+, \end{aligned} \tag{11}$$

where

$$W = \{v \in H^1(\Omega) : v = 0 \text{ on } \Gamma_d\}, \quad W_+ = \{v \in W : [v] \geqslant 0 \text{ on } \Gamma\}. \tag{12}$$

The main difficulty in the study of the above evolution variational inequality is the non-monotone dependence of f with respect to the slip $[w]$. The existence of a solution w having the regularity

$$w \in W^{1,\infty}(0,T,W) \cap W^{2,\infty}(0,T,L^2(\Omega)) \tag{13}$$

can be deduced for two-dimensional bounded domains using the method developed in [36].

3. Elliptic problem of each time step

Explicit time discretization schemes require a time step smaller than the critical CFL time step which is of the order of ratio spatial mesh size/wave velocity. The duration of the initiation phase may be very large [15,21,35] and it may not scale with the ratio characteristic length/wave speed, which means that the threshold on the time step size may be too small to allow computations of the initiation phase. That is why we need an implicit time discretization scheme allowing much larger values than the critical CFL time step.

We consider here the Newmark method, with parameters $\beta = 1/4$ and $\gamma = 1/2$ (see for instance [26]), for the time discretization of the dynamic problem (10,11). To this end, let $\Delta t > 0$ be the time step, N the maximum number of steps, and $T = N\Delta t$. We denote by $w^n, \dot{w}^n, \ddot{w}^n$ the discretization of the solution at time $t = n\Delta t$, i.e. $w^n \approx w(n\Delta t), \dot{w}^n \approx \partial_t w(n\Delta t), \ddot{w}^n \approx \partial_{tt} w(n\Delta t)$ for all $0 \leqslant n \leqslant N$. The initial conditions (10) become

$$w^0 = w_0, \quad \dot{w}^0 = w_1, \quad \ddot{w}^0 = \rho^{-1}\,\mathrm{div}(G\nabla w_0), \tag{14}$$

which is the starting point of a recursive problem. Suppose that we have constructed the solution up to $t = n\Delta t$, i.e. we have $w^k, \dot{w}^k, \ddot{w}^k$ for all $k \leqslant n$. In the Newmark method, the numerical solution $w^{n+1}, \dot{w}^{n+1}, \ddot{w}^{n+1}$ of (11) at $t = (n+1)\Delta t$ is obtained from

$$w^{n+1} = w^n + \Delta t \dot{w}^n + \frac{(\Delta t)^2}{4}(\ddot{w}^{n+1} + \ddot{w}^n), \quad \dot{w}^{n+1} = \dot{w}^n + \frac{\Delta t}{2}(\ddot{w}^{n+1} + \ddot{w}^n), \tag{15}$$

$$\begin{aligned} &\dot{w}^{n+1} \in W_+, \quad \int_\Omega \rho \ddot{w}^{n+1}(v - \dot{w}^{n+1})\mathrm{d}x + \int_\Omega G\nabla w^{n+1} \cdot \nabla(v - \dot{w}^{n+1})\mathrm{d}x \\ &\quad + \int_\Gamma f([w^{n+1}])([v] - [\dot{w}^{n+1}])\mathrm{d}\sigma \geqslant 0 \quad \forall v \in W_+. \end{aligned} \tag{16}$$

In terms of the velocity, the above problem can be written as the following variational inequality: find $\dot{w}^{n+1} \in W_+$ such that

$$\begin{aligned} &\int_\Omega \rho \dot{w}^{n+1}(v - \dot{w}^{n+1})\mathrm{d}x + \frac{(\Delta t)^2}{4}\int_\Omega G\nabla \dot{w}^{n+1} \cdot \nabla(v - \dot{w}^{n+1})\mathrm{d}x \\ &\quad + \int_\Gamma h_n([\dot{w}^{n+1}])([v] - [\dot{w}^{n+1}])\mathrm{d}\sigma \geqslant F_n(v - \dot{w}^{n+1}) \quad \forall v \in W_+, \end{aligned} \tag{17}$$

where h_n and F_n are given by

$$\begin{aligned} &h_n(x,s) = \tfrac{\Delta t}{2} f(x, [w^n](x) + ([\dot{w}^n](x) + s)\Delta t/2) \\ &F_n(v) = \textstyle\int_\Omega \rho\left(\dot{w}^n + \frac{\Delta t}{2}\ddot{w}^n\right)v\,\mathrm{d}x - \frac{\Delta t}{2}\int_\Omega G\nabla\left(w^n + \frac{\Delta t}{2}\dot{w}^n\right) \cdot \nabla v\,\mathrm{d}x. \end{aligned} \tag{18}$$

If $\dot{w}^{n+1}$ is obtained, then one can deduce w^{n+1} and $\ddot{w}^{n+1}$ through

$$w^{n+1} = w^n + \frac{\Delta t}{2}(\dot{w}^n + \dot{w}^{n+1}), \quad \ddot{w}^{n+1} = 2\frac{\dot{w}^{n+1} - \dot{w}^n}{\Delta t} - \ddot{w}^n. \tag{19}$$

The use of an implicit scheme for the wave equation with frictional type conditions on the faults will imply that we have to solve a nonlinear problem, given by a variational inequality, at each time step.

Let us put

$$\gamma = \frac{(\Delta t)^2}{4}G \tag{20}$$

and let us introduce the energy function $J_n : W \to \mathbb{R}$ given by

$$J_n(v) = \frac{1}{2}\int_\Omega \rho v^2 \,\mathrm{d}x + \frac{1}{2}\int_\Omega \gamma|\nabla v|^2 \,\mathrm{d}x + \int_\Gamma H_n([v])\mathrm{d}\sigma - F_n(v), \tag{21}$$

where H_n, which is the antiderivative of h_n, represents the density of energy dissipated on the fault during the time interval $[n\Delta t,(n+1)\Delta t]$ (see Fig. 2 for a simple diagram).

$$H_n(x,u) = \int_0^u h_n(x,s)\mathrm{d}s \quad \text{a.e. } x \in \Gamma \ \ \forall u \geqslant 0.$$

Writing $u_{n+1} = \dot{w}^{n+1}$, problem (17) becomes the following elliptic variational problem: find $u_{n+1} \in W_+$ such that

$$\int_\Omega \rho u(v-u_{n+1})\mathrm{d}x + \int_\Omega \gamma\nabla u_{n+1}\cdot\nabla(v-u_{n+1})\mathrm{d}x + \int_\Gamma h_n([u_{n+1}])([v]-[u_{n+1}])\mathrm{d}\sigma \geqslant F_n(v-u_{n+1}) \tag{22}$$

for all $v \in W_+$.

The following result can be obtained using the same technique as in [37]:

Theorem 3.1. *If $u_{n+1} \in W_+$ is a local minimum for J_n, then u_{n+1} is a solution of* (22). *Moreover there exists at least a global minimum for J_n, i.e. there exists $u_{n+1} \in W_+$ such that*

$$J_n(u_{n+1}) \leqslant J_n(v) \quad \forall v \in W_+. \tag{23}$$

Let us analyze here what are the conditions to be imposed on the parameters Δt, G, ρ and $\partial_s f$, such that the functional J_n would be strongly coercive. On this property will depend the convergence of the Schwarz algorithm described in Section 4. To this end, we have to consider the following eigenvalue problem connected to (17): find $\Phi \in W$, $\Phi \neq 0$ and $\lambda^2 \in \mathbb{R}$ such that

$$\mathrm{div}(G\nabla\Phi) = \lambda^2\rho\Phi \quad \text{in } \Omega, \tag{24}$$

$$\Phi = 0 \quad \text{on } \Gamma_\mathrm{d}, \qquad [G\partial_n\Phi] = 0, \qquad G\partial_n\Phi = g[\Phi] \quad \text{on } \Gamma, \tag{25}$$

where $g(x) = -\inf_{s\in\mathbb{R}_+}\partial_s f(x,s) = -S(x)\inf_{s\in\mathbb{R}_+}\partial_s\mu(x,s)$.

The above eigenvalue problem played a key role in the study of the nucleation phase of earthquakes (see [3,15,21,51,53]). Through the first eigenvalue, important physical properties (characteristic time, critical fault length, etc.) were deduced.

The variational formulation of the eigenvalue problem is

$$\Phi \in W, \quad \int_\Omega G\nabla\Phi\cdot\nabla v\,\mathrm{d}x + \lambda^2\int_\Omega \rho\Phi v\,\mathrm{d}x = \int_{\Gamma_f} g[\Phi][v]\mathrm{d}x \qquad \forall v \in W, \tag{26}$$

and we recall from [20] the following result:

Theorem 3.2. *Let Ω be bounded*:

(*i*) *The eigenvalues and eigenfunctions of* (24), (25) *consist of a sequence* $(\lambda_n^2,\Phi_n)_{n\in\mathbb{N}}$ with $\lambda_0^2 \geqslant \lambda_1^2 \geqslant \ldots$ *and* $\lambda_n^2 \to -\infty$.

(*ii*) *Let $\beta > 0$ and let us denote by $\lambda_0^2(\beta)$ the first eigenvalue of* (24), (25) *in which g was replaced by βg. Then $\beta \to \lambda_0^2(\beta)$ is a convex increasing function and the following inequality holds*:

$$\int_\Omega G|\nabla v|^2\,\mathrm{d}x + \lambda_0^2(\beta)\int_\Omega \rho v^2\,\mathrm{d}x \geqslant \beta\int_\Gamma g[v]^2\,\mathrm{d}x \quad \forall v \in W. \tag{27}$$

Note that, in general, λ_0^2 is not negative, hence there exist at most a finite number of positive eigenvalues.

Theorem 3.3. *Let Ω be bounded*:

(*i*) *J_n' is a Lipschitz functional, i.e. there exists a real constant b such that*

$$\|(J_n'(v_1) - J_n'(v_2))\|_{W'} \leqslant b\|v_1 - v_2\|_W. \tag{28}$$

(*ii*) *If*

$$\frac{(\Delta t)^2}{4}\lambda_0^2 < 1, \tag{29}$$

where λ_0^2 is given by the above theorem, then J_n is an uniformly convex functional, i.e. there exists $a > 0$ such that

$$J_n'(v_1)(v_1 - v_2) - J_n'(v_2)(v_1 - v_2) \geqslant a\|v_1 - v_2\|_W^2 \quad \forall v_1, v_2 \in W, \tag{30}$$

and (23) *has a unique solution which is also the unique solution of* (17), *i.e.* $u_{n+1} = \dot{w}^{n+1}$.

The above condition (29) on the time step Δt is not a CFL-type condition. If the process is stable, i.e. $\lambda_0^2 \leqslant 0$, then there is no condition (in terms of convergence and stability) on the time step. If the process is unstable, i.e. $\lambda_0^2 > 0$, then (29), which is equivalent to

$$\Delta t < \Delta t_{\mathrm{cr}} =: \frac{2}{\lambda_0}$$

is just a convergence criterion for the domain decomposition method which solves the non-quadratic minimization problem at each time step. In all the physical applications we have considered, the critical time step Δt_{cr} was found to be very large (10 up to 100 times larger than the critical CFL time step).

Proof. For $v_1, v_2, v \in W$, we get that

$$\begin{aligned}|(J_n'(v_1) - J_n'(v_2))(v)| &\leqslant \int_\Omega |\rho||v_1 - v_2||v| + \int_\Omega |\gamma||\nabla(v_1 - v_2)\cdot\nabla v| + \int_\Gamma |h_n([v_1]) - h_n([v_2])||[v]| \\ &\leqslant \|\rho\|_\infty\|v_1 - v_2\|_{L^2(\Omega)}\|v\|_{L^2(\Omega)} + \|\gamma\|_\infty\|v_1 - v_2\|_W\|v\|_W + l_h\|[v_1 - v_2]\|_{L^2(\Gamma)}\|[v]\|_{L^2(\Gamma)},\end{aligned}$$

where $l_h = L(\Delta t/2)^2$ is the Lipschitz constant of h_n. Therefore, using the continuity of the trace operator and Eqs. (4), (18) and (20), there exists a real constant b:

$$b := CL\left(\frac{\Delta t}{2}\right)^2 + \max\left\{\left(\frac{\Delta t}{2}\right)^2\|G\|_\infty, \|\rho\|_\infty\right\} \tag{31}$$

(here C is a constant) such that (28) holds. From the expression of g, we get

$$(h_n(x, s_1) - h_n(x, s_2))(s_1 - s_2) \geqslant -\eta(x)|s_1 - s_2|^2 \ \ \forall s_1, s_2 \geqslant 0 \quad \text{a.e. } x \in \Gamma, \tag{32}$$

where $\eta(x) = g(x)(\Delta t/2)^2$. After some computations, we obtain from the above inequality

$$\begin{aligned} J_n'(v_1)(v_1 - v_2) - J_n'(v_2)(v_1 - v_2) &= \int_\Omega \gamma|\nabla(v_1 - v_2)|^2\,\mathrm{d}x + \int_\Omega \rho(v_1 - v_2)^2\,\mathrm{d}x \\ &\quad + \int_\Gamma (h_n([v_1]) - h_n([v_2]))[v_1 - v_2]\mathrm{d}x \\ &\geqslant \int_\Omega \gamma|\nabla(v_1 - v_2)|^2\,\mathrm{d}x + \int_\Omega \rho(v_1 - v_2)^2\,\mathrm{d}x - \int_\Gamma \eta[v_1 - v_2]^2\,\mathrm{d}x, \end{aligned}$$

and, from (27), we get

$$(J_n'(v_1) - J_n'(v_2))(v_1 - v_2) \geqslant \frac{\beta - 1}{\beta}\int_\Omega \gamma|\nabla(v_1 - v_2)|^2\,\mathrm{d}x + \frac{\beta - \lambda_0^2(\beta)(\Delta t/2)^2}{\beta}\int_\Omega \rho(v_1 - v_2)^2\,\mathrm{d}x.$$

Bearing in mind that $\beta \to \lambda_0^2(\beta)$ is an increasing function, from (29) we get that there exists $\bar\beta > 1$ such that $\lambda_0^2(\bar\beta)(\Delta t/2)^2 < 1$, and (30) follows with

$$a = \frac{\bar\beta - 1}{\bar\beta}\min\left\{\left(\frac{\Delta t}{2}\right)^2 G_0, \rho_0\right\}. \tag{33}$$

Since the functional J_n is convex, problems (23) and (17) are equivalent. The uniqueness of u_{n+1} comes from the strict convexity of the functional J_n. □

4. Domain decomposition method

We describe in the following the domain decomposition method we have applied to solve variational inequality (22). We point out that this inequality is equivalent with the constraint minimization problem (23), in which the functional J is not quadratic. Moreover, the convex set of the constraints, W_+, is not of obstacle type for which most of the convergence results for the domain decomposition methods are obtained in the literature.

4.1. General presentation

Over the domain Ω of problem (22), we consider a regular triangular mesh $\mathscr{T}_h$ (see [17]), of mesh size h, such that the nodes on the sides of the fault Γ can be associated two by two having the same coordinates (one of them being located on a side of Γ and the other one on the other side). We shall denote in the following by x_i, $i = 1, \ldots, n_\mathrm{d}$ the interior nodes of $\mathscr{T}_h$ in Ω, and by x_i^+ and x_i^-, $i = 1, \ldots, n_f$, the pairs of nodes on the two sides of Γ having the same coordinates. We use the linear finite element spaces, and the functions in the nodal basis associated with the nodes of $\mathscr{T}_h$ will be denoted by φ_i, $i = 1, \ldots, n_\mathrm{d}$, and φ_i^+ and φ_i^-, $i = 1, \ldots, n_f$. Consequently, these basis functions will be piecewise linear, continuous functions such that: $\varphi_i(x_i) = 1$ and $\varphi_i = 0$ at the other mesh nodes of $\mathscr{T}_h$, $\varphi_i^+(x_i^+) = 1$ and $\varphi_i^+ = 0$ at the other mesh nodes of $\mathscr{T}_h$, and, finally, $\varphi_i^-(x_i^-) = 1$ and $\varphi_i^- = 0$ at the other mesh nodes of $\mathscr{T}_h$.

We shall use two decompositions of the domain Ω. The first decomposition has three subdomains, Ω_1, Ω_2 and Ω_3, and the second one has only two subdomains, Ω_1 and Ω_2. The subdomain Ω_1 is the same in the two decompositions and it contains the inner nodes of the domain, x_i, $i = 1, \ldots, n_\mathrm{d}$. The nodes x_i^+ and x_i^-, $i = 1, \ldots, n_f$, lie either in the subdomains Ω_2 and Ω_3, for the first decomposition, or in the subdomain Ω_2, for the second one. To construct these subdomains we introduce other domains, denoted O_i, which will be subdomains of Ω_1, Ω_2 and Ω_3. First, we write $O_1 = \Omega$, and we see that $x_i \in O_1$, $i = 1, \ldots, n_\mathrm{d}$. Then, for each

pair of nodes x_i^+ and x_i^- on Γ, we consider the subdomains O_{i+1}, $i = 1, \ldots, n_f$, which are obtained by the union of the triangles which have a vertex at either the node x_i^+ or the node x_i^- on Γ (see Fig. 3). Consequently, $O_{i+1} = \mathrm{Int}(\mathrm{supp}\,\varphi_i^+) \cup \mathrm{Int}(\mathrm{supp}\,\varphi_i^-)$, $i = 1, \ldots, n_f$.

Now, we introduce the first decomposition with three subdomains. In the well known coloring procedure of the subdomains, we mark with the same color the subdomains which do not intersect each other. It is easy to see the subdomains $\{O_i\}_{1 \leqslant i \leqslant M}$, $M = n_f + 1$, can be marked with three colors: the first color corresponds to O_1, and the other two colors are used for O_i, $i = 2, \ldots, n_f + 1$. Since the solutions on the subdomains having the same color can be simultaneously found, we associate to each color one subdomain: the union of the subdomains O_j having the color i will be denoted by Ω_i, i.e., $\Omega_1 = O_1$, and Ω_2 and Ω_3 are unions of subdomains O_i, $i = 2, \ldots, M$, corresponding to the second and third color, respectively. In Fig. 3, for instance, where the subdomains O_i, $i = 2, \ldots, M$ are numbered from the left end point of the fault Γ to the right one, we can take $\Omega_2 = O_2 \cup O_4 \cup O_6 \cup \cdots$ and $\Omega_3 = O_3 \cup O_5 \cup O_7 \cup \cdots$ In this way, we have obtained a new overlapping decomposition

$$\Omega = \bigcup_{i=1}^{3} \Omega_i. \tag{34}$$

The second decomposition of the domain Ω we use has only two subdomains which are written as

$$\Omega_1 = O_1 \quad \text{and} \quad \Omega_2 = \bigcup_{i=1}^{n_f} O_{i+1}. \tag{35}$$

Roughly speaking, the Schwarz algorithm is an iterative procedure in which we solve, within an iteration similar problems on each subdomain. The unknowns of such a subproblem are the unknowns of the initial problem corresponding to its subdomain. The boundary conditions of the problem on a subdomain are of Dirichlet type: the solution on a subdomain takes on the boundary the values of the solutions on the other subdomains. By the above decompositions of the domain Ω, the unknowns inside the domain and those on the boundary lie in different subdomains. Moreover, since the domain Ω_1 has no unknown on the fault, the subproblem on Ω_1 becomes a linear one, i.e. we have to solve an algebraic linear system.

In the case of the decomposition with three subdomains, the nonlinear subproblems on Ω_2 and Ω_3 are decomposed into several small independent problems of two unknowns corresponding to subdomains O_i. The fact that these nonlinear problems have only two unknowns allows us to use efficient solvers. For the decomposition with two subdomains, the nonlinear problem on Ω_2 cannot be decoupled in small independent subproblems. We have solved this subproblem by the same Schwarz algorithm in which $O_2, \ldots, O_M$ is a domain decomposition of Ω_2. In this way, we also arrive to solve nonlinear subproblems of two unknowns. Consequently, in the case of the decomposition with two subdomains, the linear system corresponding to Ω_1 is solved only after the convergence over whole Ω_2 is achieved by iterating over all O_{i+1},

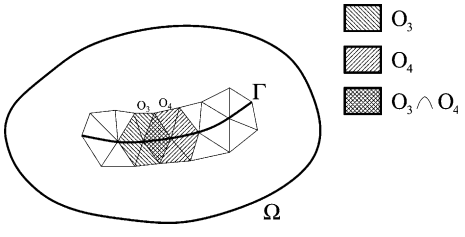

Fig. 3. Decomposition of Ω. Here, domains O_3 and O_4 have been shaded.

$i = 1, \ldots, n_f$, many times. In the case of the decomposition with three subdomains, we solve only once the nonlinear problems on O_i corresponding to Ω_2 and Ω_3, and then we solve the linear algebraic system.

As we already said, in the Schwarz algorithm, the boundary conditions of the solution in a subdomain are obtained from the values of the solutions in the other subdomains. Consequently, within an iteration, the solutions on the subdomains O_i which do not intersect each other can be simultaneously found on parallel computers. Moreover, if the iteration is made in such a way, the convergence rate of the algorithm does not depend on the number of the subdomains O_i but on the number of the subdomains Ω_i, i.e. two or three in the decompositions (35) and (34).

4.2. Multiplicative Schwarz method

We associate to the space W defined in (12) the linear finite element space

$$W^h = \{v \in C^0(\bar{\Omega}) : v_{|_\tau} \in P_1(\tau), \tau \in \mathscr{T}_h, v = 0 \text{ on } \Gamma_d\}. \tag{36}$$

Even if $\Omega_1 = \Omega$, the function subspace associated to Ω_1 will be different from W^h,

$$W_1^h = \{v \in C^0(\bar{\Omega}) : v_{|_\tau} \in P_1(\tau), \tau \in \mathscr{T}_h, v = 0 \text{ on } \partial\Omega\}. \tag{37}$$

For the domain decomposition with three subdomains, the subspaces of W^h corresponding to the subdomains Ω_2 and Ω_3 will be

$$\begin{aligned} W_2^h &= \{v \in C^0(\bar{\Omega}) : v_{|_\tau} \in P_1(\tau), \tau \in \mathscr{T}_h, v = 0 \text{ in } \Omega \setminus \Omega_2\}, \\ W_3^h &= \{v \in C^0(\bar{\Omega}) : v_{|_\tau} \in P_1(\tau), \tau \in \mathscr{T}_h, v = 0 \text{ in } \Omega \setminus \Omega_3\}, \end{aligned} \tag{38}$$

respectively. The spaces W^h and W_i^h, $i = 1, 2, 3$, are considered as subspaces of $H^1(\Omega)$. We point out that the subspace W_1^h corresponds to Dirichlet boundary conditions, and the Neumann boundary conditions corresponding to the space W^h are taken into consideration through the subspaces W_2^h and W_3^h.

The convex set W_+^h corresponding to W_+ defined in (12) is

$$W_+^h = \{v \in W^h : v(x_i^+) - v(x_i^-) \geqslant 0, i = 1, \ldots, n_f\}. \tag{39}$$

For the decomposition with two subdomains, as in the previous case, the space W^h and the convex set W_+^h are defined in (36) and (39), respectively. Also, the subspaces W_1^h and W_2^h are written as in (37) and (38), respectively. In the following we shall analyze the complexity and the convergence of the algorithm in both cases of decomposition of Ω (34) and (35). We denote by $m = 2, 3$ the number of subdomains in the decomposition.

We now assume that we have to solve inequality (22) for a given time step n, and for simplicity we shall omit the writing of this index, i.e. we shall write simply u instead of $u_{n+1} = \dot{w}^{n+1}$. In this way, the finite element form of the equivalent problems (22) and (23) are written as

$$u \in W_+^h : \int_\Omega \rho u(v-u)\mathrm{d}x + \int_\Omega \gamma \nabla u \cdot \nabla(v-u)\mathrm{d}x + \int_\Gamma h([u])([v]-[u])\mathrm{d}\sigma \geqslant F(v-u) \quad \text{for any } v \in W_+^h, \tag{40}$$

and

$$u \in W_+^h : J(u) \leqslant J(v) \quad \text{for any } v \in W_+^h, \tag{41}$$

respectively. The proposed algorithm corresponding to the subspaces $W_1^h, \ldots, W_m^h$ and the convex set W_+^h is written as a subspace correction method as follows.

Schwarz algorithm. We start the algorithm with an arbitrary $u^0 \in W_+^h$. At iteration $k+1$, having $u^k \in W_+^h$, $k \geqslant 0$, we compute sequentially for $i = 1, \ldots, m$, $r_i^{k+1} \in W_i^h$ satisfying

$$r_i^{k+1} = \arg\min_{\substack{u^{k+\frac{i-1}{m}} + v_i \in W_+^h \\ v_i \in W_i^h}} G(v_i) \quad \text{with } G(v_i) = J(u^{k+\frac{i-1}{m}} + v_i), \tag{42}$$

and then we update

$$u^{k+\frac{i}{m}} = u^{k+\frac{i-1}{m}} + r_i^{k+1}.$$

We notice that this algorithm does not assume a decomposition of the convex set W_+^h depending on the subspaces W_i^h. Problem (42) has a unique solution and it also satisfies the variational inequality

$$r_i^{k+1} \in W_i^h, u^{k+\frac{i-1}{m}} + r_i^{k+1} \in W_+^h : \left\langle J'(u^{k+\frac{i-1}{m}} + r_i^{k+1}), v_i - r_i^{k+1} \right\rangle \geqslant 0 \quad \text{for any } v_i \in W_i^h, u^{k+\frac{i-1}{m}} + v_i \in W_+^h. \tag{43}$$

As we have pointed out, in fact, inequalities (43) corresponding to $\Omega_1 = O_1$ become equations, in both cases $m = 3, 2$. Consequently, at the iteration k, we have to solve a linear algebraic system having as unknowns the corrections $r_1^{k+1} = (r^{k+1}(x_1), \ldots, r^{k+1}(x_{n_d}))$ at the nodes x_i, $i = 1, \ldots, n_d$, of $\mathscr{T}_h$ which are interior in $\Omega_1 = O_1$.

For $m = 3$, since the subdomains O_i whose union is either Ω_2 or Ω_3 are disjoint, problem (43) on either Ω_2 or Ω_3 is decomposed in several independent inequalities of two unknowns. We get such an inequality for each O_{i+1}, $i = 1, \ldots, n_f$, and the unknowns are the corrections $r^{k+1}(x_i^+)$ and $r^{k+1}(x_i^-)$ at the nodes x_i^+ and x_i^-, respectively. The solutions of these inequalities can be found by the following procedures:

(1) We first solve the system of two equations corresponding to the unconstraint minimization, finding $\tilde{r}^{k+1}(x_i^+)$ and $\tilde{r}^{k+1}(x_i^-)$, and then we write $\tilde{u}^{k+\frac{i+1}{M},+} = u^{k+\frac{i}{M},+} + \tilde{r}^{k+1}(x_i^+)$ and $\tilde{u}^{k+\frac{i+1}{M},-} = u^{k+\frac{i}{M},-} + \tilde{r}^{k+1}(x_i^-)$.
(2) If $\tilde{u}^{k+\frac{i+1}{M},+} - \tilde{u}^{k+\frac{i+1}{M},-} \geqslant 0$, we take $u^{k+\frac{i+1}{M},+} = \tilde{u}^{k+\frac{i+1}{M},+}$ and $u^{k+\frac{i+1}{M},-} = \tilde{u}^{k+\frac{i+1}{M},-}$ as the approximations at the iteration k and in the subdomain O_{i+1}, $i = 1, \ldots, n_f$, of $u(x_i^+)$ and $u(x_i^-)$, respectively.
(3) If $\tilde{u}^{k+\frac{i+1}{M},+} - \tilde{u}^{k+\frac{i+1}{M},-} < 0$, then the solution of the constraint minimization problem lies on the boundary of the convex set, i.e., $u^{k+\frac{i}{M},+} + r^{k+1}(x_i^+) = u^{k+\frac{i}{M},-} + r^{k+1}(x_i^-)$, and using it, we can find $r^{k+1}(x_i^+)$ and $r^{k+1}(x_i^-)$ by solving an unconstraint minimization problem of only one unknown.

As we have already said in the previous subsection, for $m = 2$, inequality (43) corresponding to Ω_2 contains as unknowns all the corrections $r^{k+1}(x_i^+)$ and $r^{k+1}(x_i^-)$ at the nodes x_i^+ and x_i^-, $i = 1, \ldots, n_f$. These inequalities can not be decomposed in smaller independent subproblems and, at a given iteration k, we have to find the solution simultaneously for all the unknowns corresponding to Ω_2. We have solved this inequality by the Schwarz algorithm, too, in which we have considered that $O_2, \ldots, O_{n_f+1}$ is a domain decomposition of Ω_2. Naturally, the corrections $r^{k+1}(x_i^+)$ and $r^{k+1}(x_i^-)$ corresponding to the subdomains O_i are found by the above procedures (1)–(3). In fact, the difference between the cases $m = 2$ and $m = 3$ is that in an iteration, for $m = 2$, the linear system corresponding to Ω_1 is solved only after the convergence over whole Ω_2 is achieved by iterating over all O_{i+1}, $i = 1, \ldots, n_f$, many times. For $m = 3$, in an iteration, we solve only once inequalities (43) corresponding to the subdomains O_{i+1} and then we solve the linear algebraic system.

4.3. Convergence of the method

The convergence of a general Schwarz algorithm for the minimization of convex non-quadratic functionals over a convex set in a reflexive Banach space has been given in [7]. In the case of the finite linear spaces, an error estimate for this algorithm is given in [9]. Following this result, we have:

Theorem 4.1. *For any initial $u^0 \in W_+^h$, the Schwarz algorithm converges and we have*

$$\begin{aligned} &J(u^k) - J(u) \leqslant \left(\frac{\hat{C}}{\hat{C}+1}\right)^k [J(u^0) - J(u)], \\ &\|u^k - u\|^2 \leqslant \frac{\hat{C}+1}{\bar{C}} \left(\frac{\hat{C}}{\hat{C}+1}\right)^k [J(u^0) - J(u)], \end{aligned} \tag{44}$$

where u^k are obtained from Schwarz algorithm at iteration $k \geqslant 1$, and u is the solution of problem (41). *The constants $\hat{C}$ and $\bar{C}$ are written as*

$$\hat{C} = \frac{2b}{a} m \left(1 + 2C_0 + \frac{2b}{a} m \frac{C_0^2}{\eta}\right) \frac{1}{1-\eta}, \tag{45}$$

$$\bar{C} = \frac{(2-\eta)a}{2(1-\eta)}. \tag{46}$$

In the above theorem, $m = 2, 3$ is the number of subdomains, and a and b are the constants in (33) and (31), respectively. The value of η in the expression of $\hat{C}$ and $\bar{C}$ can be arbitrary in $(0, 1)$, but there is an $\eta_0 \in (0, 1)$ such that $\hat{C}(\eta_0) \leqslant \hat{C}(\eta)$ for any $\eta \in (0, 1)$; this value η_0 can be found by solving an algebraic equation. The constant C_0 can be taken of the form

$$C_0 = C(m+1)\left(1 + \frac{m-1}{\delta}\right), \tag{47}$$

where C is independent of the mesh and domain decomposition parameters.

Since the number m of the subdomains Ω_i is in fact the number of colors of the domains O_i, in the qualitative error estimations, it can be considered as depending only on the dimension of the real space in which the domain Ω lies, i.e. it is assimilated to a constant (in general, $m \leqslant 4$ for problems in the plane). However, since the solution of the linear algebraic system corresponding to the subproblem on Ω_1 takes the most part of the computing time in an iteration, and, as our error estimate shows, the number of iterations for $m = 2$ is less than that for $m = 3$, we shall see in the numerical examples in the next section that the algorithm with two subdomains is more profitable (from the point of view of the total computing time) than that one with three subdomains.

The overlap size δ of the domain decompositions (34) and (35) is the mesh size h. Consequently, it follows from above error estimate that the number of iterations to achieve a given error is an increasing function of $1/h$.

Finally, the above theorem shows that the number of iterations is an increasing function of b/a. It follows from (31) and (33) that b is an increasing function and a is a decreasing one of the time step Δt. Consequently, the number of iterations to achieve a given error is an increasing function of Δt.

The above remarks concerning the dependence of the convergence rate on the parameters m, h and Δt will be illustrated in the next section by numerical examples. We mention that, in order to obtain a convergence rate which is independent of the mesh and domain decomposition parameters, a two- or multi-level Schwarz method (see [9]) can be applied to solve problem (41). This will be done in a subsequent paper.

5. Numerical results

The numerical results described hereafter have been chosen to reveal the characteristics of the method. Hence, the equations are handled in a non-dimensional formulation, with the rigidity G, the density ρ and the half-length of each fault segment all equal to 1. No unit is mentioned in the first two subsections. Only in the last one, where a more realistic application is considered, physical parameters have been chosen to fit

typical seismological scaling. Numerical simulations were performed using a single processor IBM RS/6000 SP Power 3-II (375 MHz). In all these simulations, $\bar{\Omega}$ is a square and Γ is a set of parallel planar cuts. The friction coefficient is piecewise linear, as suggested in (5), with D_c, S, μ_s and μ_d constant on Γ. We recall from [20] that the stability of the system is characterized by the slope of the friction law, $\beta = S[(\mu_s - \mu_d)/2D_c]$, and the fault geometry.

In the considered examples, the initial state is an unstable equilibrium position ($w \equiv 0$ with $q = -S\mu_s$) perturbed by a small velocity impulse (i.e. $w_0 \equiv 0$, $|w_1| \ll 1$). That means that the fault is at the rupture level everywhere at the initial time. The choice of this condition is motivated by two reasons. The first one is physical: we want to describe the unstable evolution of the slip near an equilibrium position. Therefore we must suppose that there exists a large enough zone on the fault where the critical strength has been reached, or will be reached in a quasi-static process. Note that the universal nucleation length for rupture instability obtained in [51] under non-uniform loading is the same that the one obtained in [21] under uniform loading. The second reason is technical: we want to point out the ability of the method in the instability capturing during the initiation phase. That is why, if the initial stress level is not at the failure level, then we need a initial perturbation w_1 with a large amplitude (of order of the slipping rate during the rupture propagation) which implies that the nucleation phase is not observed in the computed process. However, we expect qualitatively the same behavior if the fault is at an initial stress level slightly below the failure level.

The shape and location of this perturbation has no influence on the behavior of the unstable solution. However, for computational reasons, we chose it as a continuous function on Ω having a small support in the neighborhood of the fault system. The time step is chosen to satisfy (29), hence the domain decomposition method exposed in Section 4 converges at each time iteration. In this section, we denote by $\dot{w}_k^n$ the velocity at time $n\Delta t$ obtained after k Schwarz iterations. As for the stopping criterion of the iterative algorithm, it reads

$$\frac{\|\dot{w}_{k+1}^n - \dot{w}_k^n\|_2}{\|\dot{w}_{k+1}^n\|_2} \leqslant \varepsilon.$$

We chose $\varepsilon = 10^{-4}$ in all the following numerical tests.

For the sake of simplicity, the numerical examples presented in this paper concern parallel plane faults. Note that, since we use triangular meshes, the method can be applied to any system of curved faults without any difficulty.

5.1. Convergence tests for a single time step

In order to discriminate numerical errors due to the time discretization scheme from errors due to Schwarz algorithm, we first focus on the case of a single time step. In all our convergence tests, we have taken $\Gamma = [-1,1] \times \{0\}$, $\Omega = [-2,2]^2 \setminus \Gamma$ and $\beta = 1.4$. Let us remark that, since β is larger than the stability limit of a single fault $\beta_0 = 1.15777\ldots$ (see [21,51]), the equilibrium is unstable. Hence, we deal with an exponential growth of the perturbation, which is here prescribed at $t = 0$ as a velocity jump w_1 on the fault. Since we are investigating in this subsection the behavior of the solution after a single time step, we consider here a perturbation having a quite large support, taking the form of two half-Gaussians of (large) width μ and amplitude A, and applied at $t = 0$ at point $(0,0)$:

$$\begin{aligned} w_1(x_1,x_2) &= A\exp\left(\frac{x_1^2+x_2^2}{\mu^2}\right) \quad \text{if } x_2 > 0 \\ &= -A\exp\left(\frac{x_1^2+x_2^2}{\mu^2}\right) \quad \text{if } x_2 < 0. \end{aligned}$$

5.1.1. Influence of the mesh size

Computations were performed on five regular meshes described in Table 1, with $\Delta t = 0.5$. Since the mesh is regular we have taken, in this table, the length of the smallest edge instead of the usual mesh size definition.

Both decomposition methods ($m = 2$ and $m = 3$) have been tested. The number of iterations required to achieve the prescribed accuracy ($\varepsilon = 10^{-4}$) on each mesh are presented on Table 1. The first method ($m = 2$) requires 20–30% Schwarz iterations less. At each iteration, the intermediary convergence on Ω_2 requires a few iterations more (from 1 up to 8), but the computational cost of these additional calculations is negligible, so that the running time is also 20–30% smaller in the case $m = 2$. Hence, in the following, the convergence tests only concern this method.

The initial perturbation is plotted for the finest mesh (mesh 5) in Fig. 4 (left). The right part of Fig 4 shows the slip rate profile on the fault obtained after one time step, at $t = 0.5$, i.e. $[\dot{w}(0.5, x_1, 0)]$, $x_1 \in [-1, 1]$, for each of the five meshes of Table 1.

We remark that the numerical solutions are very close for meshes 3–5, which illustrates that the convergence to the continuum solution is achieved. But in terms of computation time, a very large number of nodes is expensive, as shown on Fig. 5. The number of required iterations is almost proportional to the number of nodes on Γ (as expected from the theoretical estimates of previous section), whereas the computation time of each iteration is governed by the total number of nodes. Since we are mainly interested in computing accurate approximations of the displacement and stress fields in the neighborhood of the fault, for numerical simulations involving a large number of time steps, non-regular meshes have to be used. In this way, the discretization should be fine on and around the fault, so that the local velocity distribution is well approached, but the discretization away from the fault should be coarser to reduce running times.

5.1.2. Repartition of the error

On mesh 4, Schwarz algorithm requires 27 iterations to achieve the prescribed accuracy ($\varepsilon = 10^{-4}$). The local error, defined by

$$\frac{(\dot{w}^1_{k+1}(x_1^+, 0) - \dot{w}^1_k(x_1^+, 0))^2}{\dot{w}^1_{k+1}(x_1^+, 0)^2} + \frac{(\dot{w}^1_{k+1}(x_1^-, 0) - \dot{w}^1_k(x_1^-, 0))^2}{\dot{w}^1_{k+1}(x_1^-, 0)^2}, \quad x_1 \in]-1, 1[,$$

was computed at each iteration: it concentrates on the fault, and particularly in the neighborhood of its tips (end points), where $\dot{w}$ tends to zero. It is plotted on Fig. 6 for iterations 2, 13 and 27.

Note that no error value is given at the fault tips, since $\dot{w}^{n+1}(\pm 1, 0) = 0$. The maximal local error is about 10^{-1} at iteration 2, about 10^{-3} at iteration 13, and finally about 10^{-4} at iteration 27. As expected, the relative local error is maximal at the fault tips, due to singularities of the exact solution and due to the fact that $\dot{w}^1_{k+1}$ tends to zero. In conclusion, the approximation is satisfactory along the fault, but the error due to singularities ought to be handled by other discretization techniques.

Table 1
Convergence tests for the Schwarz method with 2 and 3 subdomains

Mesh	Mesh size (h)	Number of nodes	Number of edges on the fault	Number of iterations	
				$m = 2$	$m = 3$
1	0.5	90	4	4	5
2	0.2	490	10	8	11
3	0.1	1858	20	13	19
4	0.05	7240	40	27	36
5	0.025	29459	80	50	65

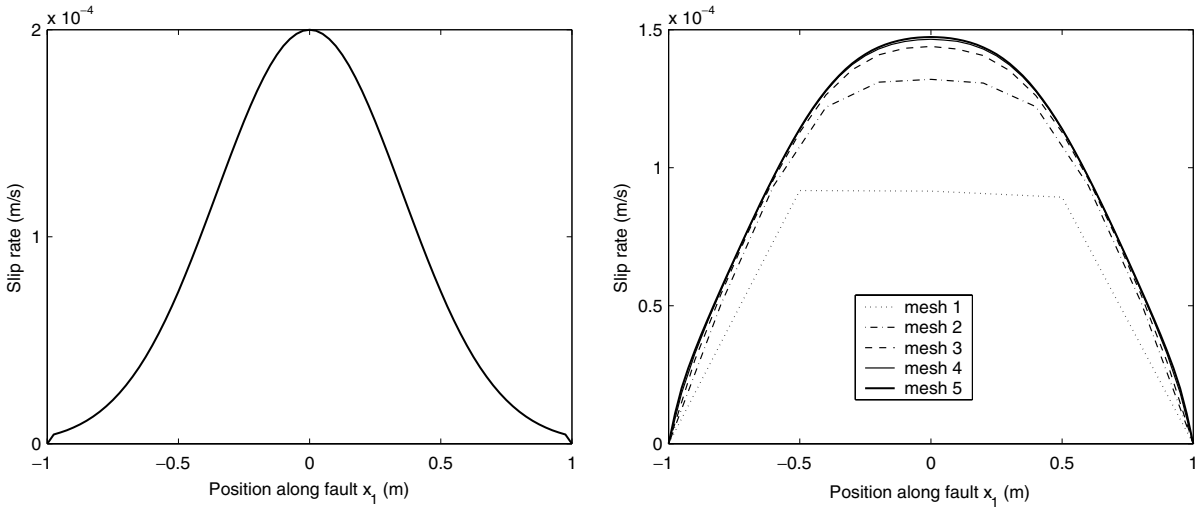

Fig. 4. Left: velocity jump $[w_1]$ on the fault at $t = 0$. Right: velocity jump after one time step ($\Delta t = 0.5$).

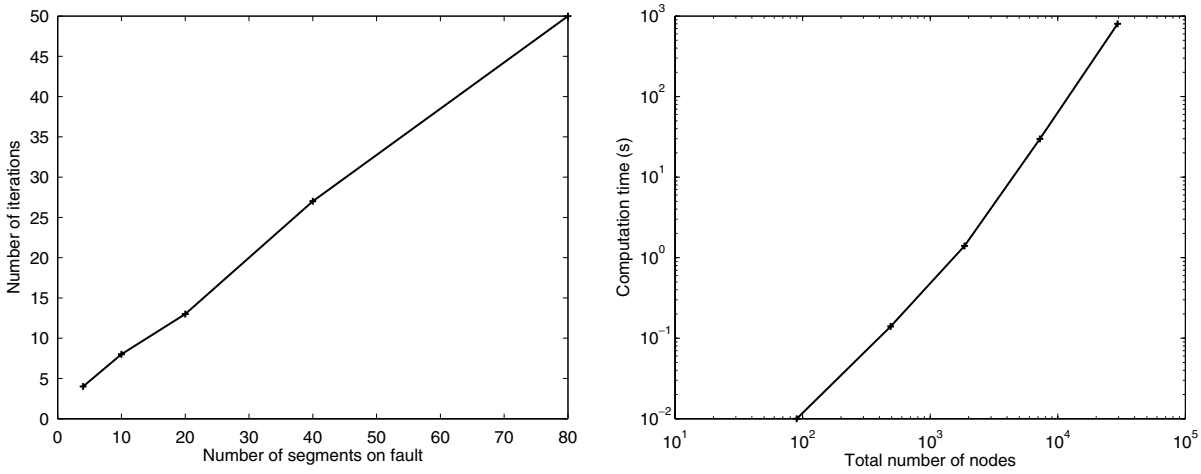

Fig. 5. Left: number of iterations vs. fault discretization. Right: logarithm of computation time vs. logarithm of mesh size.

5.1.3. Influence of the time step

The dependence of the convergence rate on the time step size has been tested using mesh 4. As stated at the end of previous section, the number of iterations is expected to be an increasing function of the time step. One can see on Fig. 7 that this was confirmed by the numerical experiments, since the number of iterations is almost proportional to Δt.

When simulating the evolution of the system for a long period of time, a small value of Δt would guarantee a small number of iterations per time step. But the total computation time is also proportional to the total number of time steps, hence inversely proportional to Δt. In conclusion, the optimal value of Δt depends on the whole evolution process. This point will be discussed later.

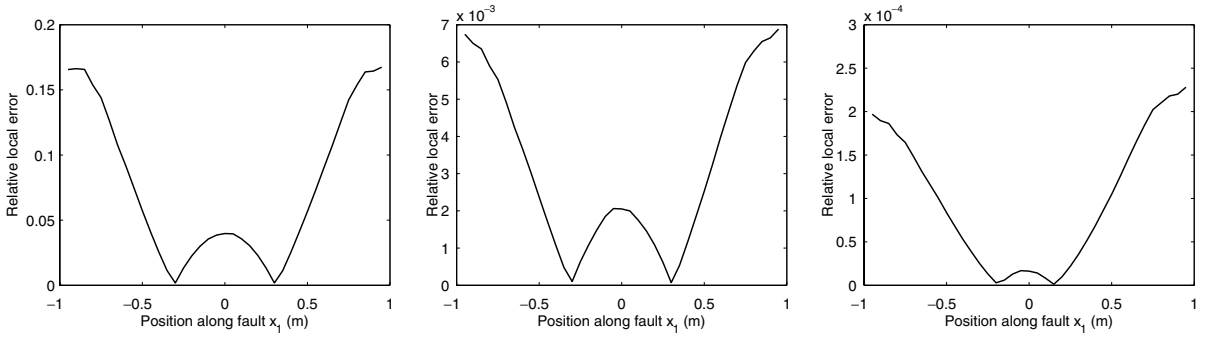

Fig. 6. Relative local error on the fault at iterations 2, 13 and 27 (the final iteration), computed on mesh 4. Note that it is not defined at $x = \pm 1$.

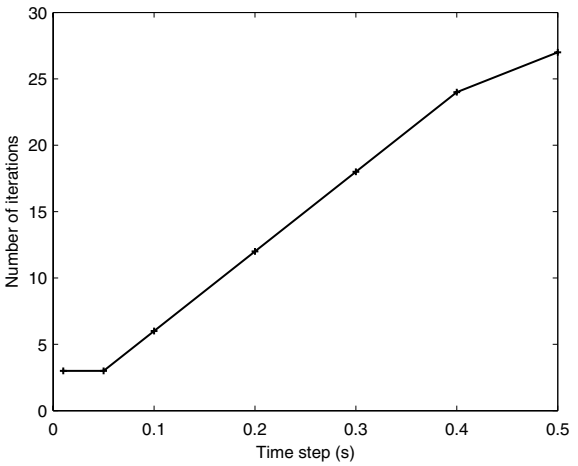

Fig. 7. Number of iterations vs. Δt for a single time step on mesh 4.

5.2. Convergence in time

To get a numerical simulation on the time interval $[0, T]$ with $T = 5$, computations on several successive time steps were performed on a heterogeneous mesh, with 6996 nodes and 40 edges on the fault. As it follows from Fig. 4, this mesh is fine enough to give a satisfactory approximation of the solution around the fault. A small velocity perturbation (a Gaussian with small width μ and small amplitude A) is applied at $t = 0$ at the fault center:

$$w_1(x_1, x_2) = A \exp\left(\frac{x_1^2 + x_2^2}{\mu^2}\right).$$

The evolution of the system is observed for 6 different values of Δt: 0.5, 0.2, 0.1, 0.05, 0.02 and 0.01. The friction parameter is $\beta = 3.0$.

Here, we aim at showing that our numerical method is able to handle exponentially growing solutions, such as the characteristic solution of the initiation phase of earthquakes. For this purpose, the critical slip D_c was taken infinite. This remark is important to understand the huge values of slip rate that we obtain.

5.2.1. Instability capturing

Fig. 8 shows the evolution of the logarithm of the slip rate at fault center, i.e. $t \to \log([\dot{w}(t,0,0)])$. The evolution is fast (due to the large value of β, here 3.0), and the slip rate at fault center is exponentially growing. The linear shape of $t \to \log([\dot{w}(t,0,0)])$ is expected during the initiation phase of instabilities (e.g. [21]). Indeed, $\dot{w}(t) \simeq \text{Const}\, e^{\alpha_0 t}\Phi_0$, where α_0, Φ_0 are the first eigenvalue and eigenfunction of problem (24), (25). The three smallest time steps ($\Delta t = 0.05$, $\Delta t = 0.02$ and $\Delta t = 0.01$) lead to quasi-identical profiles. This shows that the numerical algorithm based on Newmark time scheme and Schwarz method is efficient in capturing time instabilities, when the solution has an exponential time growth. Indeed, the Newmark scheme with parameters $\beta = 1/4$, $\gamma = 1/2$, also called average acceleration method, is known to be unconditionally stable and non-dissipative. It only leads to some dispersion for large time steps.

5.2.2. Energy conservation

Fig. 9 investigates the energy dissipation of the numerical algorithm. The test consists in considering the evolution of the sum of potential energy, kinetic energy and frictional energy, i.e.

$$\mathscr{E}(t) = \mathscr{E}_{\mathrm{c}}(t) + \mathscr{E}_{\mathrm{p}}(t) + \mathscr{E}_{w}(t) = \int_{\Omega} \rho(\dot{w}(t)^2 - w_1^2)\mathrm{d}x + \int_{\Omega} G|\nabla w(t)^2|\mathrm{d}x - \int_{\Gamma} F([w(t)])\mathrm{d}\sigma,$$

where F is the antiderivative of f. On Fig. 9, $\mathscr{E}$ is renormalized by the final value of $\mathscr{E}_{\mathrm{c}} + \mathscr{E}_{\mathrm{p}}$. Theoretically, $\mathscr{E}$ should be constant. We remark that the numerical scheme is strongly conservative: the normalized final value of $\mathscr{E}$ is smaller than the error criterion $\varepsilon = 10^{-4}$ multiplied by the number of time steps. Hence, Schwarz method is dissipative, but this dissipation can be controlled by the choice of the error criterion.

5.2.3. Optimal time step

The time step is a very important parameter, not only in terms of stability and accuracy of the solution, but also in terms of computation time. Concerning the accuracy, the above results imply that any time step smaller than or equal to 0.05 gives satisfactory approximations. Running times of these computations are plotted on Fig. 10. Obviously, they are governed by the total number of Schwarz iterations needed to compute the entire period of time $[0, 5s]$. Indeed, a small value of Δt would imply a large number of time steps, but the corresponding number of Schwarz iterations at each time step is small (see the previous

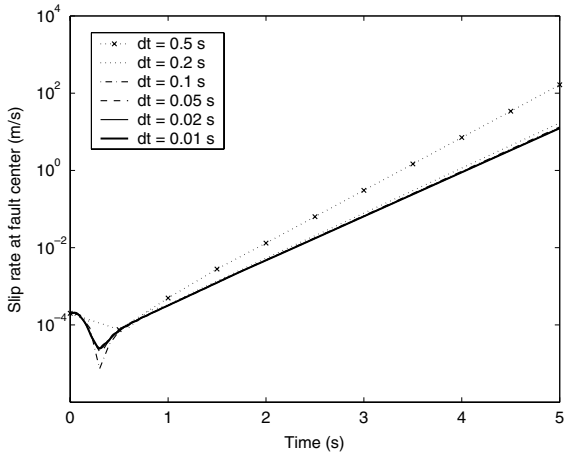

Fig. 8. Evolution of the logarithm of the slip rate at fault center, for six different values of Δt. Note that the numerical scheme is efficient in capturing unstable solutions (with an exponential growth in time).

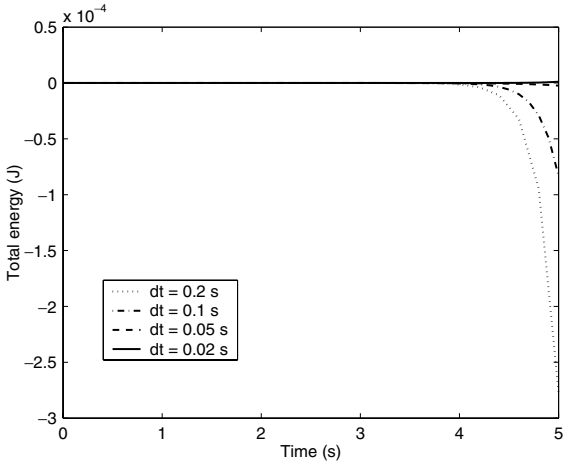

Fig. 9. Evolution of the renormalized total energy, for the 4 intermediary values of Δt.

subsection). For $\Delta t < 0.05$, the average number of Schwarz iterations is approximately the same, 4, so that computation times blow up for small time steps. Then, the average number of Schwarz iterations is 4 for $\Delta t = 0.05$ (100 time steps), 7 for $\Delta t = 0.1$ (50 time steps), 18 for $\Delta t = 0.2$ (25 time steps), so that the total number of iterations is almost the same, approximately 400. Finally, for $\Delta t = 0.5$, the average number of iterations is 90, so that the computation time is much larger. Hence, the optimal time step to minimize computation times is between 0.05 and 0.2. Since, as far as accuracy is concerned, it should not exceed 0.05, then in this particular case (irregular mesh with the smallest edge size equal to 0.05), the optimal value seems to be $\Delta t = 0.05$.

5.3. Application to interacting parallel fault segments

Rupture change, delays and/or arrest due to stress interaction on parallel or perpendicular fault segments have been investigated a lot in the last decade. In [29–33,42], spontaneous dynamic rupture is modeled using

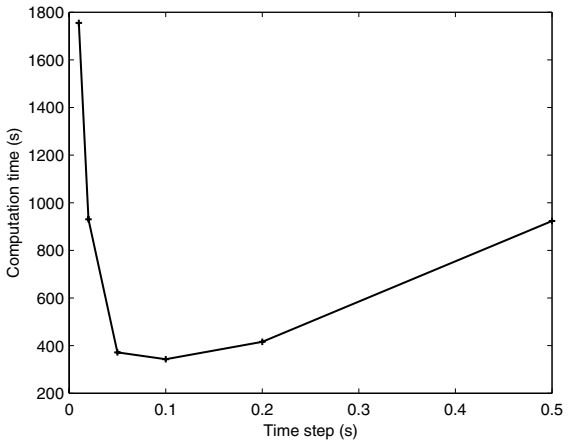

Fig. 10. Graph of the computation time of a simulation in the time period $T = 5$ plotted against Δt.

finite difference schemes and slip weakening friction. In [55], a critical strain fracture criterion is used to investigate small-scale crack interaction. However in these works, the simultaneous nucleation of rupture (weakening process) on non-coplanar interacting faults is never considered. We want to point out in this subsection that the method presented in this paper fully handles this complex situation, where the weakening process strongly interacts with fault segmentation.

We investigate here the rupture nucleation and propagation on two interacting parallel faults Γ_1 and Γ_2 represented in Fig. 11. The parameters are chosen to be physically relevant: $\rho = 2800$ kg/m^3, $c = 3$ km/s and $D_c = 0.5$ m. We deduce $G = 25.2$ GPa and a typical strength drop $S(\mu_s - \mu_d) = 5.04$ MPa. The two parallel fault segments are $\Gamma_1 = [-15\text{ km}, 5\text{ km}] \times \{-1\text{ km}\}$ and $\Gamma_2 = [-5\text{ km}, 15\text{ km}] \times \{1\text{ km}\}$. We chose $\Omega = [-50\text{ km}, 50\text{ km}]^2 \setminus \Gamma_1 \setminus \Gamma_2$, $\beta = 2.0$ and $\Delta t = 0.09$ s. The mesh has 6938 nodes, and 66 edges on each fault. A velocity perturbation (a gaussian with width μ and amplitude A) is applied at $t = 0$ at an arbitrary point, here $(x_1^0, x_2^0) = (1\text{ km}, 0\text{ km})$:

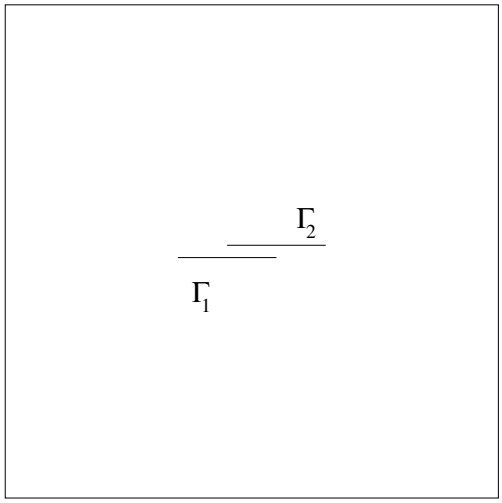

Fig. 11. Geometry of the two-faults system.

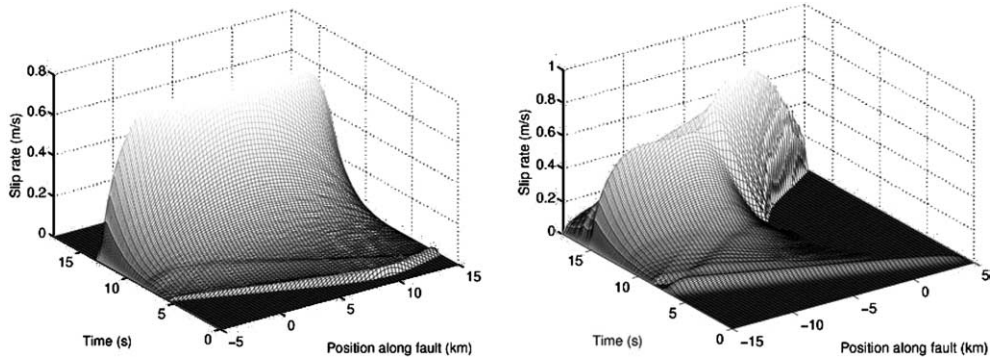

Fig. 12. Slip rate evolution on two interacting parallel faults (left: Γ_1, right: Γ_2).

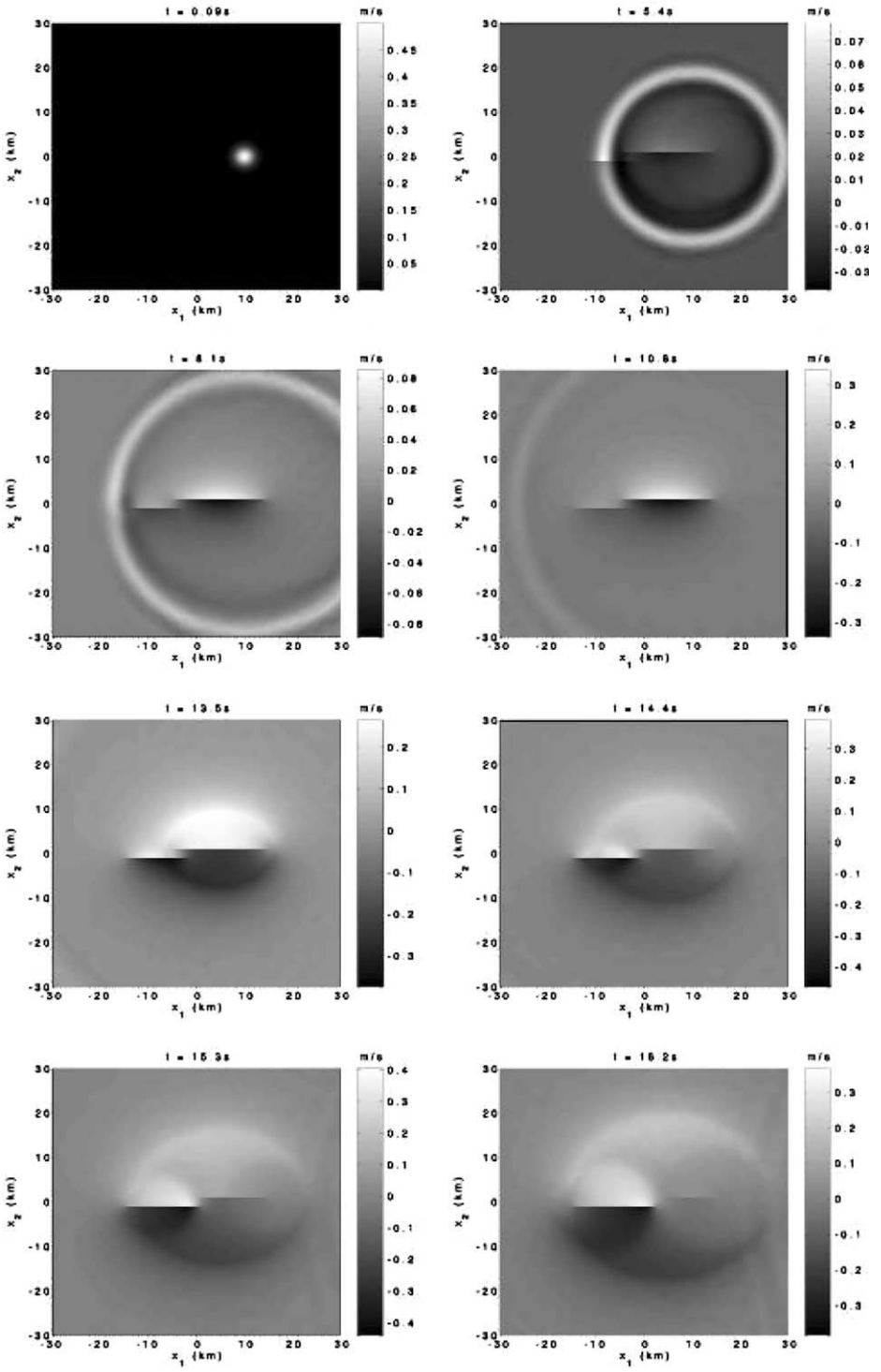

Fig. 13. Evolution of the velocity field on two interacting parallel faults.

$$w_1(x_1, x_2) = A \exp\left(\frac{(x_1 - x_1^0)^2 + (x_2 - x_2^0)^2}{\mu^2}\right).$$

Also, we chose $\mu = 2$ km together with a quite large value of the amplitude $A = 0.05$ m/s, so that the simulation can rapidly show both the initiation and rupture phases in a short period of time.

Fig. 12 displays the evolution of the velocity jump on the fault system, for $0\ \text{s} \leqslant t \leqslant 18$ s. On Fig. 13, one can see the entire velocity field for different values of t between 0.09 and 16.2 s. Note that the exterior boundary is not visible on Fig. 13. Since no absorbing boundary condition is used, there are some artificial reflections, but they do not reach the faults during the modeled time period.

The perturbation propagates in the elastic medium and first reaches Γ_2. It propagates along Γ_2 and is finally reflected by the fault tips. Slip occurs rapidly on the entire fault segment. On Γ_1, once the perturbation has propagated from the right tip to the left one, we can see a reflected wave coming from the left tip of Γ_2. Slip also initiates on Γ_1 is also perturbed, but the previous slip event on Γ_2 has already induced a stress drop on its neighborhood. A significant part of Γ_1 is inhibited for a while, because the static friction level cannot be overcome. Such interaction between the fault segments is responsible for the asymmetric velocity profile of Γ_1 during the initiation, with a single stress singularity and a locked zone (stress shadow). The characteristic global initiation pattern dominates on snapshots 3 and 4, with the slip rate growing exponentially, such that the remaining waves cannot be seen any longer. As the slip grows exponentially, it finally reaches the critical value $2D_c$, close to the center of Γ_2, which is the condition for the beginning of rupture propagation (snapshot 5). Because of the shadow zone created by the slip on Γ_2, rupture is delayed on Γ_1 and will be forced to propagate backwards on the inhibited part (snapshots 7 and 8), once the critical slip value is reached at some point of the ''initiated'' part.

This example shows that, if an initiation process (a precursory slip) occurs on a fault system, it significantly modifies the conditions under which the rupture will propagate: one of the faults is partly locked, which breaks the geometrical symmetry, and the locked part can break later, with a local directivity which is opposed to the global rupture directivity. Although this mechanism has been noticed about rupture, we show here that it can take place at a very early stage of the rupture process, i.e. during initiation or precursory slip, which is a regime in-between statics and strong dynamics.

6. Conclusion

We have presented in this paper a numerical method able to capture exponentially growing solutions of a wave propagation problem with slip-dependent interface conditions on a system of faults with complex geometry. Convergence is achieved for time steps quite larger than the usual CFL limit. Numerical tests show that the method is unconditionnally stable, with some numerical dissipation that can be controled by the error criterion of the iterative process. The number of Schwarz iterations is an increasing function of both the time step and the mesh size (a multilevel Schwarz method could make the number of iterations independent of the mesh size). The application of this method to a system of two simultaneously nucleating faults shows that the numerical scheme is able to handle complex expressions of fault interaction, i.e. both shadow zones and stress singularities.

Acknowledgements

We want to thank the two anonymous reviewers for their comments and their suggestions which helped us improve this paper.

References

[1] B. Aagaard, Finite-element simulations of earthquakes, Ph.D. Thesis, California Institute of Technology, Pasadena, 2000.
[2] J.-P. Ampuero, Etude physique et numérique de la nucléation des séismes, Ph.D. Thesis, Institut de Physique du Globe, Paris, 2002.
[3] J.-P. Ampuero, J.-P. Vilotte, F.J. Sanchez-Sesma, Nucleation of rupture under slip dependent friction law simple models of fault zone, J. Geophys. Res. 107 (B12) (2002) 101029–101043.
[4] R. Archuleta, G. Frazier, Three-dimensional numerical simulations of dynamic faulting in a half-space, Bull. Seism. Soc. Am. 68 (1978) 541–572.
[5] H. Aochi, E. Fukuyama, Three-dimensional nonplanar simulation of the 1991 Landers earthquake, J. Geophys. Res. 107 (2001), 10.1028/2000JB000032.
[6] L. Badea, On the Schwarz alternating method with more than two subdomains for nonlinear monotone problems, SIAM J. Numer. Anal. 28 (1991) 179–204.
[7] L. Badea, Convergence rate of a multiplicative Schwarz method for strongly nonlinear inequalities, in: V. Barbu, I. Lasiecka, D. Tiba, C. Varsan (Eds.), Analysis and Optimization of Differential Systems, Kluwer Academic Publishers, Boston, 2003, pp. 31–42.
[8] L. Badea, X.-C. Tai, J. Wang, Convergence rate analysis of a multiplicative Schwarz method for variational inequalities, SIAM J. Numer. Anal. 41 (3) (2003) 1052–1073.
[9] L. Badea, Convergence rate of a Schwarz multilevel method for the constraint minimization of non-quadratic functionals, SIAM J. Numer. Anal. (2003), submitted.
[10] E. Bécache, P. Joly, C. Tsogka, Fictitious domains mixed finite elements and perfectly matched layers for elastic 2D wave propagation, J. Comput. Acoust. 9 (3) (2001) 1175–1203.
[11] E. Bécache, P. Joly, C. Tsogka, A new family of mixed finite elements for the linear elastodynamic problem, SIAM J. Numer. Anal. 39 (6) (2002) 2109–2132.
[12] C. Bernardi, Y. Maday, Spectral, spectral element and mortar element methods, in: J. Blowey, J. Coleman, A. Craig (Eds.), Theory and Numerics of Differential Equations. Proc. of the 9th EPSRC Numerical Analysis Summer School, Univ. of Durham, GB, July 10–21, 2000, Springer Universitext., Berlin, 2001, pp. 1–57.
[13] A. Bizzari, M. Cocco, D.J. Andrews, E. Boschi, Solving the dynamic rupture with different numerical approaches and constitutive laws, Geophys. J. Int. 144 (2001) 656–678.
[14] M. Bouchon, D. Streiff, Propagation of a shear crack on a nonplanar fault: a method of calculation, Bull. Seism. Soc. Am. 87 (1997) 61–66.
[15] M. Campillo, I.R. Ionescu, Initiation of antiplane shear instability under slip dependent friction, J. Geophys. Res. 122 (B9) (1997) 20363–20371.
[16] T.F. Chan, T.P. Matew, Domain decomposition algorithms, Acta Numer. (1994) 61–143.
[17] P.G. Ciarlet, The Finite Element Method for Elliptic Problems, North-Holland, Amsterdam, 1978.
[18] A. Cochard, R. Madariaga, Dynamic faulting under rate-dependent friction, Pageoph 142 (1994) 419–445.
[19] S. Das, K. Aki, A numerical study of two-dimensional spontaneous rupture propagation, Geophys. J. R. Astronom. Soc. 50 (1977) 643–668.
[20] C. Dascalu, I.R. Ionescu, Slip weakening friction instabilities: eigenvalue analysis, Math. Models Methods Appl. Sci. (M3AS) 3 (14) (2004) 439–459.
[21] C. Dascalu, I.R. Ionescu, M. Campillo, Fault finiteness and initiation of dynamic shear instability, Earth Planetary Sci. Lett. 177 (2000) 163–176.
[22] W.L. Elsworth, G.C. Beroza, Seismic evidence for an earthquake nucleation phase, Science 268 (1995) 851–855.
[23] P. Favreau, M. Campillo, I.R. Ionescu, Initiation of inplane shear instability under slip dependent friction, Bull. Sism. Soc. Am. 89 (5) (1999) 1280–1295.
[24] P. Favreau, M. Campillo, I.R. Ionescu, Initiation of instability under slip dependent friction in three dimension, J. Geophys. Res. 107 (B7) (2002), art. no. 2147.
[25] E. Fukuyama, R. Madariaga, Integral equation method for plane crack with arbitrary shape in 3D elastic medium, Bull. Seism. Soc. Am. 85 (1995) 614–628.
[26] T.C. Fung, Unconditionally stable higher order Newmark methods by sub-stepping procedure, Comput. Methods Appl. Mech. Eng. 147 (1997) 61–84.
[27] P. Geubelle, J. Rice, A spectral method for 3D elastodynamic fracture problems, J. Mech. Phys. Solids 43 (1995) 1791–1803.
[28] R. Glowinski, G.H. Golub, G.A. Meurant, J. Périeux (Eds.), First Int. Symp. on Domain Decomposition Methods, SIAM, Philadelphia, 1988.
[29] R.A. Harris, R.J. Archuleta, S.M. Day, Fault steps and the dynamic rupture process – 2-D numerical simulations of a spontaneously propagating shear fracture, Geophys. Res. Lett. 18 (1991) 893–896.
[30] R.A. Harris, S.M. Day, Dynamics of fault interaction – parallel strike-slip faults, J. Geophys. Res. 98 (1993) 4461–4472.
[31] R.A. Harris, S.M. Day, Dynamic 3D simulations of earthquakes on en echelon faults, Geophys. Res. Lett. 26 (1999) 2089–2092.

[32] Y. Kase, K. Kuge, Numerical simulation of spontaneous rupture processes on two non-coplanar faults: the effect of geometry on fault interaction, Geophys. J. Int. 135 (1998) 911–922.
[33] Y. Kase, K. Kuge, Rupture propagation beyond fault discontinuities: significance of fault strike and location, Geophys. J. Int. 147 (2001) 330–342.
[34] Y. Iio, Slow initial phase of the P-wave velocity pulse generated by microearthquakes, Geophys. Res. Lett. 19 (5) (1992) 477–480.
[35] I.R. Ionescu, M. Campillo, The influence of the shape of the friction law and fault finiteness on the duration of initiation, J. Geophys. Res. 104 (B2) (1999) 3013–3024.
[36] I.R. Ionescu, Q.-L. Nguyen, S. Wolf, Slip dependent friction in dynamic elasticity, Nonlinear Anal. 53 (3–4) (2003) 75–390.
[37] I.R. Ionescu, J.-C. Paumier, On the contact problem with slip dependent friction in elastostatics, Int. J. Eng. Sci. 34 (4) (1996) 471–491.
[38] D. Komatitsch, J. Tromp, Introduction to the spectral-element method for 3-D seismic wave propagation, Geophys. J. Int. 139 (1999) 806–822.
[39] D. Komatitsch, J.P. Vilotte, The spectral element method: an efficient tool to simulate the seismic response of 2-D and 3-D geological structures, Bull. Seism. Soc. Am. 88 (1998) 368–392.
[40] D. Komatitsch, J.P. Vilotte, R. Vai, J.M. Castillo-Covarrubias, F.J. Sanchez-Sesma, Spectral element approximation of elastic waves equations: application to 2-D and 3-D seismic problem, Int. J. Numer. Methods Eng. 45 (1999) 1139–1164.
[41] P. Le Tallec, Domain decomposition methods in computational mechanics, in: J. Tinsley Oden (Ed.), Computational Mechanics Advances, 1 (2), North-Holland, Amsterdam, 1994, pp. 121–220.
[42] H. Magistrale, S. Day, 3D Simulations of multi-segment thrust fault rupture, Geophys. Res. Lett. 26 (14) (1999) 2093–2096.
[43] R. Madariaga, K. Olsen, R. Archuleta, Modeling dynamic rupture in a 3D earthquake model, Bull. Seism. Soc. Am. 88 (1998) 1182–1197.
[44] D. Oglesby, Earthquake dynamics on dip-slip faults, Ph.D. Thesis, University of California, Santa Barbara, 1999.
[45] D. Oglesby, R. Archuleta, S. Nielsen, Dynamics of dip-slip faulting: explorations in two dimensions, J. Geophys. Res. 105 (2000) 13643–13653.
[46] D. Oglesby, S. Day, The effect of fault geometry on the 1999 Chi–Chi (Taiwan) earthquake, Geophys. Res. Lett. 28 (2001) 1831–1834.
[47] M. Ohnaka, Y. Kuwakara, K. Yamamoto, Constitutive relations between dynamic physical parameters near a tip of the propagation slip during stick-slip shear failure, Tectonophysics 144 (1987) 109–125.
[48] A. Quarteroni, A. Valli, Domain Decomposition Methods for Partial Differential Equations, Oxford Science Publications, 1999.
[49] B.F. Smith, P.E. Bjørstad, W. Gropp, Domain Decomposition: Parallel Multilevel Methods for Elliptic Differential Equations, Cambridge University Press, Cambridge, 1996.
[50] C. Tsogka, Modélisation mathématique et numérique de la propagation des ondes élastiques tridimensionnelles dans des milieux fissurés, Ph.D. Thesis, Université de Paris IX Dauphine, 1999.
[51] K. Uenishi, J. Rice, Universal nucleation length for slip-weakening rupture instability under non-uniform fault loading, J. Geophys. Res. 108 (B1) (2003) ESE17-1–ESE17-14, cn:2042, doi:10.1029/2001JB001681.
[52] J. Virieux, R. Madariaga, Dynamic faulting studied by a finite difference method, Bull. Seisol. Soc. Am. 72 (1982) 345–369.
[53] S. Wolf, I. Manighetti, M. Campillo, I.R. Ionescu, Mechanics of normal fault networks subject to slip weakening friction, submitted.
[54] J. Xu, J. Zou, Some nonoverlapping domain decomposition methods, SIAM Rev. 40 (1998) 857–914.
[55] T. Yamashita, Y. Umeda, Earthquake rupture complexity due to dynamic nucleation and interaction of subsidiary faults, PAGEOPH 143 (1994) 89–115.